Quantum Science and Technology

PAPER

Quantum sensing of the electron electric dipole moment using ultracold entangled Fr atoms

T Aoki[1,2,3,*], R Sreekantham[4,5], B K Sahoo[4], Bindiya Arora[6], A Kastberg[7], T Sato[1], H Ikeda[1], N Okamoto[1], Y Torii[1], T Hayamizu[3], K Nakamura[8], S Nagase[8], M Ohtsuka[3], H Nagahama[8], N Ozawa[8], M Sato[1], T Nakashita[1], K Yamane[1], K S Tanaka[9], K Harada[9], H Kawamura[9], T Inoue[9], A Uchiyama[9], A Hatakeyama[10], A Takamine[3], H Ueno[3], Y Ichikawa[11], Y Matsuda[1], H Haba[3] and Y Sakemi[8]

[1] Institute of Physics, Graduate School of Arts and Sciences, The University of Tokyo, Tokyo 153-8902, Japan
[2] PRESTO, Japan Science and Technology Agency (JST), Kawaguchi 332-0012, Japan
[3] RIKEN Nishina Center for Accelerator-Based Science, Wako, Saitama 351-0198, Japan
[4] Atomic, Molecular and Optical Physics Division, Physical Research Laboratory, Ahmedabad-380009, India
[5] Department of Physics, Indian Institute of Technology, Gandhinagar, Gujarat-382355, India
[6] Department of Physics, Guru Nanak Dev University, Amritsar, Punjab-143005, India
[7] Institute de Physique de Nice, Université Côte d'Azur, CNRS, 06108 Nice, France
[8] Center for Nuclear Study, The University of Tokyo, Wako, Saitama 351-0198, Japan
[9] Cyclotron and Radioisotope Center, Tohoku University, Sendai, Miyagi 980-8578, Japan
[10] Department of Applied Physics, Tokyo University of Agriculture and Technology, Tokyo 184-8588, Japan
[11] Department of Physics, Kyushu University, Fukuoka 819-0395, Japan
[*] Author to whom any correspondence should be addressed.

E-mail: aoki@phys.c.u-tokyo.ac.jp

Keywords: quantum sensing, quantum entanglement, spin squeezing, electron electric dipole moment, laser cooling, atom interferometry

OPEN ACCESS

RECEIVED
5 March 2021

REVISED
4 August 2021

ACCEPTED FOR PUBLICATION
6 August 2021

PUBLISHED
10 September 2021

Abstract

We propose a method to measure the electron electric dipole moment (eEDM) using ultracold entangled francium (Fr) atoms trapped in an optical lattice, yielding an uncertainty below the standard quantum limit. Among the alkali atoms, Fr offers the largest enhancement factor to the eEDM. With a Fr based experiment, quantum sensing using quantum entangled states could enable a search for the eEDM at a level below 10^{-30} *e*cm. We estimate statistical and systematic errors attached to the proposed measurement scheme based on this quantum sensing technique. A successful quantum sensing of the eEDM could enable the exploration of new physics beyond the standard model of particle physics.

1. Introduction

The electron electric dipole moment (eEDM), arising due to parity and time-reversal symmetry violating (P, T-odd) interactions, is a subtle physical property. The potential confirmation and quantitative determination discovery of the eEDM is likely to shed light on new physics beyond the standard model (SM) of particle physics [1, 2]. Although efforts to measure the eEDM have been pursued for more than 40 years, it has not yet been observed. However, experimental efforts to narrow down its possible range are steadily gaining ground. The current status is that the experimental uncertainties are about ten orders of magnitude larger than the value predicted by the SM. A further reduction of the uncertainties in eEDM measurements will advance the constraining of proposed models beyond the SM.

On account of the enhanced effects, heavy open-shell atoms and polar molecules are considered as the most promising candidates to observe eEDM. At present, the best limit on eEDM comes from the thorium oxide (ThO) experiment, at $|d_e| < 1 \times 10^{-29}$ *e*cm, with 90% confidence [3]. However, eEDM is not the only P, T-odd interaction source that contributes to the measurement. The scalar–pseudoscalar (S–PS) electron–nucleus interactions are also the other P, T-odd interaction that contribute significantly. To

separate out these contributions, it is imperative to perform experiments on more than one system. Owing to the fact that inferring the S–PS interaction contributions from the complex molecules is a tedious procedure, measurements in atoms are better for such purposes. Till date, the best experimental limit using atoms comes from ^{205}Tl [4]. The other atom where measurement is available is ^{133}Cs [5, 6] (see also reference [6]). However, ^{210}Fr atom has the largest enhancement factor due to eEDM (about 1.5 and 7 times larger than Tl and Cs atoms respectively) and a recent theoretical study has highlighted its advantageous features for analyzing both the eEDM and S–PS contributions from its measurement [7].

The measurement of the eEDM is typically performed by polarizing an atom or a molecule in a beam experiment with an applied external electric field. Compared to molecules, atoms require application of large electric field owing their spherical symmetric structure. The interaction time with the electric field in a beam experiment is limited to a few milliseconds, because atoms in an atomic beam and molecules in a molecular beam transit through the interaction region in a short time. Thus, it is possible to improve the statistical uncertainties in these experiments by increasing the interaction time of atoms or molecules with the applied electric field.

It is well known today that very high-precision measurements are achievable using the laser cooled atoms have been well studied for many high-precision measurements. This is why it is natural to expect that the next-generation experiments to measure eEDM can be based on such cold atoms or molecules. In fact, some of the recent studies have demonstrated how laser cooled and trapped atoms or molecules can be suitable in prolonging the interaction time up to 10 s to measure eEDM [8–14]. The principle to measure the eEDM using trapped molecular ions has also been reported [15, 16], but the statistical sensitivity in the measurements using ions can be limited by the number of ions, which can be interrogated due to strong Coulomb repulsion among them. Laser cooled neutral atoms can be extended to an eEDM measurement so as to increase the interaction time by confining atoms in an optical lattice [17]. However, to improve the current upper limit for the eEDM a prerequisite is to significantly improve the sensitivity of the experiment. This limit is restricted by the standard quantum limit (SQL) as $1/\sqrt{N}$, where N is the total number of atoms or molecules used in the experiment.

To overcome the limitations of earlier methods applied in eEDM measurements, we propose a novel experimental technique to measure eEDM using ultracold atoms based on the combined principles of quantum sensing and optical lattice to circumvent the limitation over atom–electric field interaction time. The underlying principle of this technique is that it uses quantum states as sensors and/or detectors to measure physical quantities. Depending on the working mechanism, quantum sensor techniques are broadly classified into three types [18]: type I involving quantum states, type II based on quantum coherence, and type III that uses entangled quantum states to beat the SQL. Recently, as a proof-of-principle experiments, the stabilities of the Rb microwave (MW) atomic clock [19] and the Yb optical atomic clock [20] have surpassed the SQL using the quantum entangled states. It is, therefore, promising to exploit the quantum entanglement in quantum sensing to overcome the limitations in the measurement of the eEDM below the SQL.

As a proof-of-principle study, we consider ultracold entangled Fr atoms trapped in an optical lattice to carry out an eEDM measurement with an uncertainty below the SQL. As mentioned above, Fr has the largest eEDM enhancement factor among other considered atoms for the experiment. In our proposed approach, we suggest employing an optical cavity method to create a squeezed state of collective spins (Bloch vectors) as entangled quantum states. Quantum sensing with the entangled states will enable us to search for the eEDM to below 10^{-30} $e$cm. Thereby, it will surpass the current best reported limit on eEDM and will be able to probe the signatures of new physics beyond the SM. We also estimate typical systematics associated with such measurement by performing high-accuracy calculations of the static and dynamic second-order and hyperfine-induced third-order dipole polarizabilities of the ground state of ^{210}Fr atom.

The paper is organized as follows. In section 2, we describe the measurement method of the eEDM using atomic squeezed states in Fr atoms trapped in an optical lattice. In section 3, we present results for the energy shifts calculated in the experimental scheme, and cancellations of them are discussed. We end the article with a conclusion.

2. Measurement method of eEDM using the spin-squeezed state

We discuss here the quantum sensing using atomic squeezed states, technique for the eEDM measurement in an optical lattice, and the detection procedure using the squeezed spin state (SSS). Finally, we estimate the possible uncertainties in the eEDM measurement using the aforementioned methods.

One typical measurement method for eEDM is the Ramsey resonance. Let us consider the phase difference θ of the atomic wave function between the ground and excited states. The phase uncertainty of

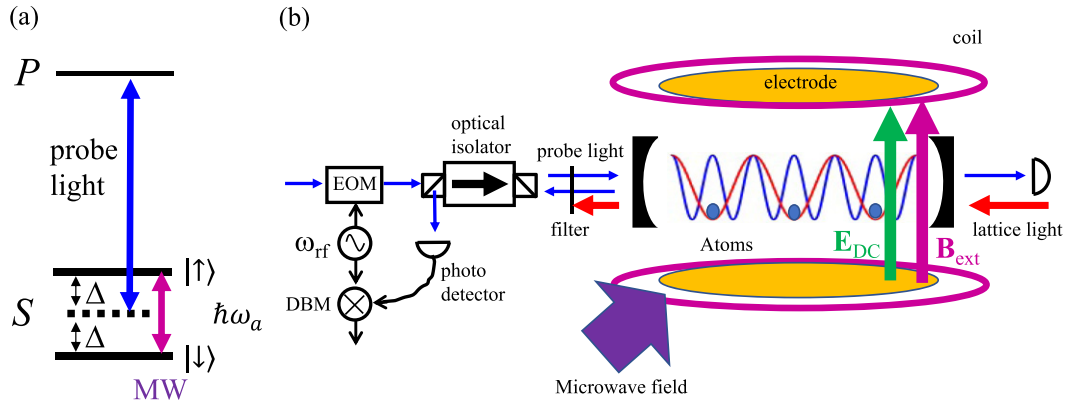

Figure 1. Energy diagram and experimental setup for the atom–light interaction proposed to create the SSS. (a) Energy diagram and related transitions in the atom. The detuning of the probe light is set to the midpoint of the hyperfine splitting in the S state. A MW field is resonant between the hyperfine states of $|\uparrow\rangle$ and $|\downarrow\rangle$. (b) Lattice light creates a trap potential in the cavity, which atoms are trapped at anti-nodes. The peak of the probe light overlaps with the atoms in the optical lattice. The atoms will feel close to maximum intensity at the anti-node of the probe standing wave. The probe beam in introduced to the optical cavity through an electro-optical modulator (EOM) and an optical isolator in order to enable stabilisation through the Pound–Drever–Hall (PDH) technique [48]. Reflected probe light is monitored on a photo detector (PD). An electric field $\mathbf{E}_{\rm DC}$ is generated by a pair of the electrodes, and a magnetic field $\mathbf{B}_{\rm ext}$ by a pair of Helmholtz coils. DBM: double-balanced mixer.

the Ramsey resonance $\delta\theta$ is:

$$\delta\theta = 1/\sqrt{N}, \tag{1}$$

where N is the total number of atoms. This is the so called 'SQL' or shot noise limit [21]. If a k-particle entanglement state exists in the N particle atomic ensemble, the uncertainty of equation (1) is improved as a bound for metrologically useful state as [22]

$$\delta\theta = 1/\sqrt{kN}. \tag{2}$$

For $k = N$, equation (2) gives the so called 'Heisenberg limit' ($\delta\theta = 1/N$). Several kinds of entangled states may decrease the detection limit below the SQL [18, 22]. One of these is the SSS.

The SSS of atoms was first proposed by Kitagawa and Ueda [23] that shows the net interaction is proportional to square of the collective spin of the atoms. This interaction using Faraday rotation of light was also shown in [24]. As an applications of SSS for atomic clocks, Wineland *et al* [25, 26] discussed the squeezed Bloch vector in a Ramsey resonance in order to decrease the uncertainty of the signal [26]. By interacting with the square of spins via collisions, the reduction of the uncertainty using the SSS to below the SQL have been demonstrated for a Bose Einstein condensate [27].

On the other hand, Kuzmich *et al* [28] and Takahashi *et al* [29] have suggested measurements based on the use of linearly polarized light. In experiments, the uncertainties in the case of SSS have been shown to reach below the SQL in Yb [30] and Cs [31] by using the above method. Lately, the squeezing gain of ultracold Rb has been enhanced by using an optical cavity [32, 33]. The SSS for more than 10^5 Rb atoms in an optical lattice improved the stability of the MW atomic clock transition in a proof-of-principle experiment [19]. Recently, it has been shown that the SSS improved stability of the Yb optical lattice clock [20]. This suggests that carrying out an eEDM measurement by generating the SSS in an optical cavity can boost its precision to an unprecedented level.

First, we consider a three-level atom interacting with monochromatic probe light, as shown in figure 1(a). The optical frequency is detuned midway between the hyperfine levels $|\uparrow\rangle$ and $|\downarrow\rangle$ with the detuning $\Delta = \omega_a/2$, where ω_a is the hyperfine splitting between the $|\uparrow\rangle$ and $|\downarrow\rangle$ states. The states $|\uparrow\rangle$ and $|\downarrow\rangle$ are coupled with a MW field to enable the Ramsey resonance experiment. The atom is prepared in an optical cavity with a resonance frequency ω_c, which corresponds to the light frequency (figure 1(b)). Atoms are trapped at anti-nodes of the standing wave produced by the superposed lattice beam inside the cavity. The probe beam is generated by frequency doubling of the lattice light. The wavelengths for the probe and lattice lights are 718 nm and 1436 nm, respectively. The peak of the probe light's standing wave enfolds the atoms in the optical lattice of the cavity as shown in figure 1(b). In this configuration, the probe light is approximately uniformly coupled to all atoms [19]. In the following discussion of atom–light interaction, we omit the effect of the lattice light. The electric field $\mathbf{E}_{\rm DC}$ generated by a pair of electrodes and the magnetic field $\mathbf{B}_{\rm ext}$ applied by a pair of Helmholtz coils will be affecting the atoms (figure 1(b)).

The Hamiltonian ($H_{\rm EDM}$) representing the interaction of atomic electric dipole moment (EDM) with an electric field is given by

$$H_{\rm EDM} = -\mathbf{d}_{\rm atom} \cdot \mathbf{E}_{\rm DC}, \tag{3}$$

where $\mathbf{d}_{\rm atom} = R\mathbf{d}_{\rm e}$ is the atomic dipole moment, $\mathbf{d}_{\rm e}$ the eEDM, and R is the enhancement factor. It to be noted that R is proportional to Z^3, where Z is the atomic number. Since the Fr atom has the largest Z among the alkali metals, and it has been laser cooled and trapped [34–38], it makes the most suitable atom for the experimental consideration. The R value of Fr has been calculated earlier [39] and its the most accurate value is reported as $R = 799$ [7]. Using $\mathbf{d}_{\rm e} = d_{\rm e}\mathbf{J}/\hbar$ and the Wigner–Eckart theorem gives the expectation value of $\langle d_{\rm e}\rangle$ as

$$\begin{aligned}\langle \mathbf{d}_{\rm e}\rangle &= \frac{d_{\rm e}}{\hbar}\frac{\langle \mathbf{J}\cdot\mathbf{F}\rangle}{F(F+1)}\langle \mathbf{F}\rangle \\ &= \frac{d_{\rm e}}{\hbar}\frac{F(F+1)+J(J+1)-I(I+1)}{2F(F+1)}\langle \mathbf{F}\rangle \\ &\simeq d_{\rm e}(g_F/g_J)\langle \mathbf{F}\rangle/\hbar,\end{aligned} \tag{4}$$

where $\mathbf{J}$ the electron angular momentum, $\mathbf{I}$ the nuclear spin, and the total atomic angular momentum is $\mathbf{F} \equiv \mathbf{J} + \mathbf{I}$. F, J, and I are the respective quantum numbers. g_J and g_F are Landé g-factors for $\mathbf{J}$ and $\mathbf{F}$. In an alkali atom, the ground state $S_{1/2}$ is split into two hyperfine states $F = I + 1/2$ and $F = I - 1/2$. For ^{210}Fr, the nuclear spin is $I = 6$. The quantization axis z is fixed by the direction of the applied electric field $\mathbf{E}_{\rm DC}(x, y, z) = (0, 0, E_{\rm DC})$, and equation (3) becomes

$$H_{{\rm EDM},F,M_F} = -Rd_{\rm e}(g_F/g_J)\mathbf{F}\cdot\mathbf{E}_{\rm DC}/\hbar = -(g_F/g_J)Rd_{\rm e}M_F E_{\rm DC}, \tag{5}$$

where M_F is the magnetic quantum number of F, $g_F/g_J = 1/13$ for the $7S_{1/2}$, $F = 13/2$ state, and $-1/13$ for the $7S_{1/2}$, $F = 11/2$ state. To detect the energy shift in equation (5), an MW field resonant between $F = 13/2$ and $F = 11/2$ state is applied to the trapped atoms. The frequency difference from the hyperfine splitting is given by

$$\Delta\omega_{\rm EDM} \equiv \Delta\omega_{\rm EDM}^{M_F', M_F} \equiv \frac{g_F' M_F' - g_F M_F}{g_J\hbar} Rd_{\rm e}E_{\rm DC}. \tag{6}$$

Next, we consider the Hamiltonian of atoms interacting with probe light. Taking into account the cavity resonance frequency $\omega_{\rm c}$ and probe light inside the cavity, the Hamiltonian can then be written as [40]

$$H = \hbar\left(\omega_{\rm c} + \Delta\omega_{\rm c}\right)\hat{c}^\dagger\hat{c} + \hbar\omega_a J_{a,z}, \tag{7}$$

where $\Delta\omega_{\rm c}$ is the shift of the cavity resonance frequency due to the refractive indices of atoms in the $|\uparrow\rangle$ and $|\downarrow\rangle$ states, $\hat{c}^\dagger$ ($\hat{c}$) are the creation (annihilation) operators of intra cavity photons of probe light. If we define the $\mathbf{j}_a$ as the optical Bloch vector for the $|\uparrow\rangle$ and $|\downarrow\rangle$ states of a single atom, with magnitude 1/2, $\mathbf{J}_a = \Sigma\mathbf{j}_{a,i}$ is the summation of the atomic Bloch vectors for N atoms, $J_{a,z}$ the z component of $\mathbf{J}_a$, and $J_a = |\mathbf{J}_a| = N/2$ the magnitude of $\mathbf{J}_a$. The first and second terms in equation (7) correspond to the total photon energy and the third term is the total atomic energy for N atoms. As the detuning Δ is tuned to the midpoint between the $|\uparrow\rangle$ and $|\downarrow\rangle$ states (figure 1(a)), the light feels the dispersion of atoms as a positive refractive index in the $|\uparrow\rangle$ state and a negative one in the $|\downarrow\rangle$ state. The AC Stark shift $\Delta\omega_{\rm c}$ is written as

$$\Delta\omega_{\rm c} = \frac{2g^2}{\Delta}\frac{N_+ - N_-}{2} = \frac{2g^2}{\Delta}J_{a,z}, \tag{8}$$

where $2g$ is the single-photon Rabi frequency in the transition between the S and P states, and N_+ (N_-) the number of atoms in the $|\uparrow\rangle$ ($|\downarrow\rangle$) state. Then, equation (8) is written as

$$H = \hbar\omega_{\rm c}\hat{c}^\dagger\hat{c} + \hbar\frac{2g^2}{\Delta}\hat{c}^\dagger\hat{c}J_{a,z} + \hbar\omega_a J_{a,z}. \tag{9}$$

After the interaction of the probe light with atoms inside the cavity, corresponding to the second term in equation (9), the measurement of probe light results in the quantum nondemolition (QND) measurement of the atomic collective spin $\mathbf{J}_a$.

In references [28, 29], creation of the SSS using a QND measurement of an atomic collective spin is proposed based on the Hamiltonian $H_{\rm QND} = \chi S_z J_{a,z}$, where the χ is the coefficient, and the S_z is one of the Stokes parameters for the probe light [29]. During the interaction of light and atom through $H_{\rm QND}$, $\mathbf{S}$ precesses around the z axis by an angle $kJ_{a,z}$ with $k = \chi t/\hbar$ and t is the interaction time. The interaction gives as the lowest order, $S_y^{\rm out} \approx S_y^{\rm in} + kS_x^{\rm in}J_{a,z}^{\rm in}$. Its variance is $(\Delta S_y^{\rm out})^2 = (n/4)(1+\kappa^2) = (n/4)\xi^2$ with the

photon number n, $\xi^2 = (1+\kappa^2)$, and $\kappa^2 = nNk^2/4$ [22, 42]. After the measurement of S_y, the variance of J_z is given by $(\Delta J_{a,z}^{\rm out})^2 = (N/4)/\xi^2 = (N/4)/(1+\kappa^2)$. Although $(\Delta S_y^{\rm out})^2$ is larger than the variance in the coherent state of probe light $n/4$, $(\Delta J_{a,z}^{\rm out})^2$ is smaller than the variance of coherent spin state (CSS) $N/4$. Thus, it demonstrates that the $\mathbf{J}$ is in the SSS.

The squeezing process through the measurement of probe light from the cavity due to the interaction of the probe light with $\mathbf{J}_{a,z}$ in the optical cavity, as given by equation (9), is described in detail in reference [41, 43, 44]. The variance of this squeezed spin $\Delta J_{a,z}$ is written as

$$(\Delta J_{a,z})^2 = \xi_{\rm R}^2 (\Delta J_{z,\rm CSS})^2, \tag{10}$$

where $\xi_{\rm R}$ is the Wineland parameter. Following equation (10), the variance $(\Delta J_{a,z})^2$ can be smaller than that in the CSS $(\Delta J_{z,\rm CSS})^2 = J_a/2 = N/4$ if $\xi_{\rm R}$ is smaller than one. By considering the photon shot noise and Raman scattering process, $\xi_{\rm R}$ can be given for the squeezing in the optical cavity as [22, 44]:

$$\xi_{\rm R}^2 = \frac{1 + 4NC(\Gamma/\omega_a)^2}{\sqrt{qNC/p}}, \tag{11}$$

where $C = (2g)^2/(\kappa\Gamma)$ is the single-atom cavity cooperativity, κ the linewidth of the optical cavity, Γ the natural line width of the transition between the S and P states, and q the quantum efficiency of the photo detector (PD) monitoring probe light and the whole efficiency to detect the probe light [44]. The parameter p represents the probability for a free-space photon scattering event causes an atom to spin flip from $|\uparrow\rangle$ to $|\downarrow\rangle$ via the intermediate state $|e\rangle$. The fluctuations of N_+ and N_- due to the spin-flip via this Raman process are anti-correlated. For instance, if $\mathbf{J}_a = (N/2)\hat{x}$, the N_+ value can decrease while the N_- value can increase via the Raman process. As a result, it will increase $(\Delta J_{a,z})^2$ because of the fact that $J_{a,z} = (N_+ - N_-)/2$. Thus, lower p value is desired for achieving smaller $\xi_{\rm R}$ value for our requirement.

To measure the energy shift of equation (6) using the SSS generated by the Hamiltonian of equation (9), we utilize the Ramsey resonance technique in the SSS [25, 26] with an optical cavity [19, 20, 31, 33, 43–46].

We consider the following experimental steps:

(a) We have to prepare suitable states for the EDM measurement, with the latter consisting of two steps, as shown in figure 2. First, the atoms are laser cooled in a magneto-optical trap (MOT). Next, they are cooled by polarization-gradient cooling, and are loaded into the optical lattice in the cavity (figure 1(b)). Then, the atoms are further cooled by Raman sideband cooling into the vibrational ground state [47]. At this stage, the atoms are initially populated in the states $7S_{1/2}$, $F = 13/2$ and $F = 11/2$. We take the total number of atoms as $2N$. Second, the atoms are optically pumped into the $7S_{1/2}, F = 11/2, M_F = 11/2$ and $M_F = -11/2$ by irradiating them with light resonant to the transition between $7S_{1/2}, F = 11/2$ and $7P_{3/2}, F' = 9/2$, and at the same time light resonant with $7S_{1/2}, F = 13/2$ and $7P_{3/2}, F' = 13/2$, with both pump beams having π polarization (figure 2(a)). Next, the magnetic field is applied and the population in the $7S_{1/2}, F = 11/2, M_F = -11/2$ is adiabatically transferred to $7S_{1/2}, F = 13/2, M_F = -11/2$ by sweeping the MW field resonant with the hyperfine transition in the Zeeman shifted hyperfine states (figure 2(b)). The atoms are in the binary mixture of N atoms in the $7S_{1/2}, F = 11/2, M_F = 11/2$, and N atoms in $7S_{1/2}, F = 13/2, M_F = -11/2$ states. These state are useful to cancel additional frequency shifts. The additional frequency shifts and the cancellation mechanism are discussed in section 3.

(b) We consider a timing sequence for the MW and probe light pulses, as shown in figure 3. After the preparation of the atomic state in (a), the atoms are in the binary mixture of the $7S_{1/2}, F = 11/2$, $M_F = 11/2$ and $7S_{1/2}, F = 13/2, M_F = -11/2$ states, as shown in figure 3(a). We considers two Bloch vectors $\mathbf{J}_{-M}$ for the $M_F = -11/2$ between $S_{1/2}, F = 13/2$ and $F = 11/2$, and $\mathbf{J}_{+M}$ for the $M_F = 11/2$ between $S_{1/2}, F = 13/2$ and $F = 11/2$ states, with isotropic uncertainties $\Delta J_{\pm M,x} = \Delta J_{\pm M,y} = \Delta J_{\pm M,z} = \sqrt{N}/2$ in the CSS, as shown in figure 3(c). The Bloch vectors in figure 3(c) are $\mathbf{J}_{+M} = -(N/2)\hat{z}$, and $\mathbf{J}_{-M} = +(N/2)\hat{z}$. Then, the MW $\pi/2$ pulse with a duration of τ is applied to rotate the Bloch vectors around the y axis (figures 3(c) and (d)).

(c) Following references [33, 46] for the generation of the SSS, the probe light pulse, the MW π pulse, and the probe light pulse are applied separately, as shown in figure 3(b).

The PDH signal [48] is obtained by measuring the probe light reflected from the cavity [49], as shown in figure 1(b). The probe light has a linear polarization parallel to the external electric and magnetic fields for π transitions. Its frequency is tune to near the transition between $7S_{1/2}$ and $7P_{3/2}$ states and the detuning is tuned to the midpoint between the $7S_{1/2}, F = 13/2$ and $7S_{1/2}, F = 11/2$ states (figure 3(a)), The probe light is reflected by the cavity is separated from the incident beam by the polarization-beam splitter in the optical isolator, and is then detected by the photo detector (PD). After the signal is demodulated in the

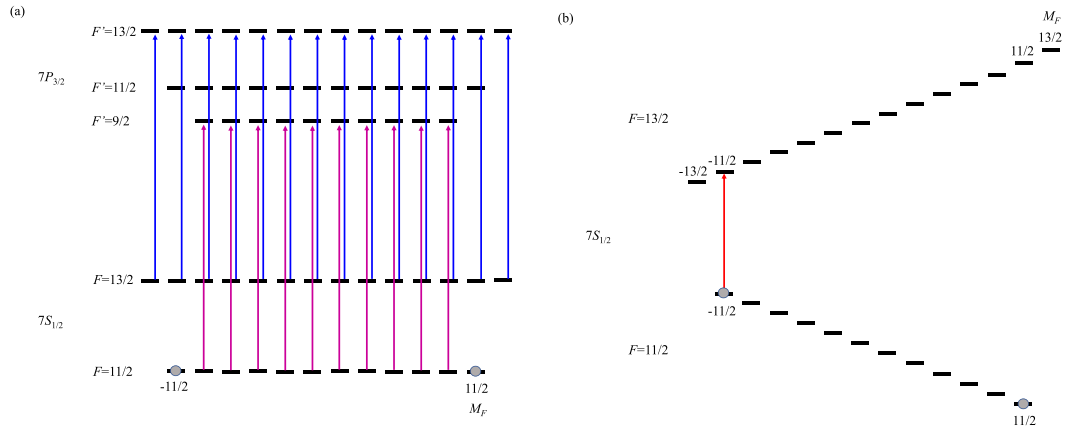

Figure 2. Energy diagram and related transitions for state preparations. (a) Optical pumping of atoms into the $7S_{1/2}$, $F = 11/2$, $M_F = 11/2$ and $M_F = -11/2$ states. (b) Adiabatic transfer from $7S_{1/2}$, $F = 11/2$, $M_F = -11/2$ to $7S_{1/2}$, $F = 13/2$, $M_F = -11/2$ states by sweeping the MW frequency with the magnetic field.

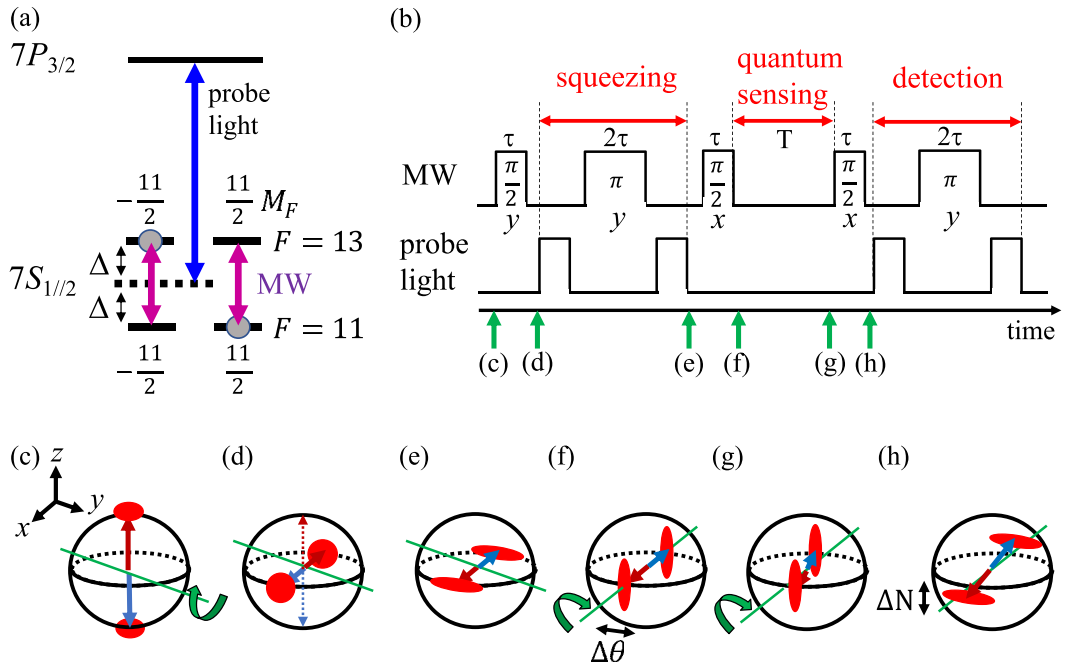

Figure 3. A five-level atom with spin one-half, timing sequence for the MW and the probe-light pulses, and Bloch vectors for collective spins. (a) Atomic distributions after the initializing, as shown in figure 2. The frequency of probe light is tuned to the middle point of the hyperfine splitting between $F = 13/2$ and $F = 11/2$ states. (b) Timing sequence for the MW and probe light pulses. The notation $\pi/2$ (π) with τ (2τ) and x (y) refers to the $\pi/2$ (π) rotation around the axis of x (y) of Bloch vectors. (c)–(h) Bloch vectors (red and blue arrows) on the Bloch spheres with uncertainty ellipsoids (red) during the squeezing and the Ramsey resonance process. Red (blue) arrows represent the Bloch vector $\mathbf{J}_{-M}$ ($\mathbf{J}_{+M}$) for the $S_{1/2}, F = 13/2, M_F = -11/2(11/2)$ and $F = 11/2, M_F = -11/2(11/2)$. (c) Bloch vectors after the initialization (figure 2) with isotropic uncertainties in the CSS. (d) Bloch vectors after rotation around the x axis. (e) Bloch vectors are squeezed after the measurement. (f) and (g) Bloch vectors during the quantum sensing of eEDM in Ramsey resonance. (h) Final Bloch vectors for the measurement.

double-balanced mixer (DBM) with the modulation frequency $\omega_{\rm rf}$ for the electro-optical modulator (EOM), as shown in figure 1(b), the dispersion signal is obtained. As the cavity resonance frequency of the signal is shifted proportional to the atom number difference $N_+ - N_-$ due to equations (7)–(9), the probe light frequency is tuned to the cavity resonance. As a result of the measurement of the probe light, the uncertainties of the Bloch vectors $\Delta J_{+M,z}$ and $\Delta J_{-M,z}$ are reduced for the time indicated by the arrows (d) and (e) in figure 3(b). The spatially inhomogeneous light shifts of the $S_{1/2}, F = 13/2$ and $F = 11/2$ states induced by the probe light results in decoherence of the Bloch vectors. To avoid this, the MW π pulse is applied in a spin-echo technique (see supplemental material in reference [46]).

(a) The MW $\pi/2$ pulse, with a temporal phase of 90 degree compared to the preceding MW field, is applied as a first pulse of Ramsey resonance. The MW pulse rotates the Bloch vector around the x axis with an angle of $\pi/2$ and a duration of τ. After the interrogation time T for the quantum sensing of eEDM, the final MW $\pi/2$ pulse with a duration of τ and a phase φ is applied and it rotates the Bloch vector around the x axis again. The final $J_{\pm M,z}$, which corresponds to the uncertainty of the number of atoms ΔN, is measured by again detecting the reflected probe light.

In the steps (b) and (c), the PDH signals are measured as the frequency shift $\Delta\omega_c$ of the dispersion curve by the existence of atoms. The $\Delta\omega_c$ in equation (8) obtained through the dispersion curve gives us the $J_{a,z}$=$(N_+ - N_-)/2$ in the case of figure 1(a). In figure 3(a), $\Delta\omega_c$ gives $J_{+M,z} + J_{-M,z}$, where $J_{\pm M,z}$ are the z components of $J_{\pm M}$.

Finally, as a result of the Ramsey resonance, $J_{+M,z}$ is $(N/2)\sin(\Delta\omega_{+M}T - \varphi)$, and $J_{-M,z}$ is $(N/2)(-\sin(\Delta\omega_{-M}T - \varphi))$. If the final MW pulse has a phase of $\varphi = 0$, $J_{+M,z}$ and $J_{-M,z}$ are written as

$$J_{+M,z} = \frac{N}{2}\sin(\Delta\omega_{+M}T) \tag{12}$$

$$J_{-M,z} = -\frac{N}{2}\sin(\Delta\omega_{-M}T), \tag{13}$$

where $\Delta\omega_{\pm M}$ are

$$\Delta\omega_{\pm M} \equiv \left(\Delta E_{F=13/2,\pm M} - \Delta E_{F=11/2,\pm M}\right)/\hbar - \omega_{MW}, \tag{14}$$

$\Delta E_{F=13/2,\pm M}$ ($\Delta E_{F=11/2,\pm M}$) is the energy in the $7S_{1/2}$, $F = 13/2$, $M_F = \pm M$ ($7S_{1/2}$, $F = 11/2$, $M_F = \pm M$) state, and $\omega_{\rm MW}$ is the MW frequency between the $7S_{1/2}$, $F = 13/2$ and $7S_{1/2}$, $F = 11/2$ states.

We define $\omega_{\rm HFS}$ as the resonant frequency between $7S_{1/2}$, $F = 13/2$ and $F = 11/2$ states with neither the Stark shift nor the Zeeman shift. The ω_{MW} is tuned to near the $\omega_{\rm HFS}$. If $1/\tau$ (τ, the interaction time of the MW field) is much larger than $\Delta\omega_{\pm M}$, this monochromatic MW field induces two transitions as shown in figure 3(a): the transition from $7S_{1/2}$, $F = 11/2, M_F = 11/2$ to $7S_{1/2}$, $F = 13/2, M_F = 11/2$ states and the transition from $7S_{1/2}$, $F = 13/2, M_F = -11/2$ to $7S_{1/2}$, $F = 11/2, M_F = -11/2$ states. Therefore, equation (14) include only the frequency shift from $\omega_{\rm HFS}$ as

$$\Delta\omega_{\pm M} = \omega_{\rm HFS} + \Delta\omega_{{\rm EDM},\pm M} - \omega_{\rm MW}, \tag{15}$$

where

$$\Delta\omega_{{\rm EDM},\pm M} \equiv \Delta\omega_{\rm EDM}^{\pm M,\pm M}. \tag{16}$$

The signal S obtained is $J_{+M,z} + J_{-M,z} = (N_{F=13/2,M_F=11/2} - N_{F=11/2,M_F=11/2})/2 + (N_{F=13/2,M_F=-11/2} - N_{F=11/2,M_F=-11/2})/2$. Thus, it can be written as

$$S = J_{+M,z} + J_{-M,z}. \tag{17}$$

As the frequency shift of the eEDM is very small, equation (17) is approximately written as

$$\begin{aligned} S &\sim \frac{N}{2}(\Delta\omega_{+M} - \Delta\omega_{-M})T \\ &= \frac{N}{2}(\Delta\omega_{{\rm EDM},+M} - \Delta\omega_{{\rm EDM},-M})T. \end{aligned} \tag{18}$$

If we assume $d_e = 1 \times 10^{-29} e$cm, $E_{\rm DC} = 100$ kV cm^{-1}, $M_F^{'} = 11/2$, and $M_F = 11/2$, equation (18) gives $(\Delta\omega_{{\rm EDM},+M} - \Delta\omega_{{\rm EDM},-M})/2\pi = 326$ nHz.

After repeated measurements, taking into account equations (6) and (18) and the frequency uncertainty of SQL from reference [26], the uncertainty of the EDM at the SQL, using the CSS $\delta d_e^{\rm CSS}$, is written as

$$\delta d_e^{\rm CSS} = \frac{13\hbar}{22RE_{\rm DC}}\frac{1}{\sqrt{NTt_{\rm total}}}, \tag{19}$$

where $t_{\rm total} = mT$ is the total interrogation time over all the measurement, and m is the number of measurements. $N = 2.5 \times 10^5$ for trapped Fr atoms, as reported in reference [51], and $t_{\rm total} = 1$ day $= 24$h $= 86\,400$ s, then equation (19) gives $\delta d^{\rm CSS} = 3.3 \times 10^{-29}$ $e$cm. For $t_{\rm total} = 10$ days, $\delta d^{\rm CSS} = 1.0 \times 10^{-29}$ $e$cm.

On the other hand, using the SSS with $\xi_{\rm R}$ (equation (11)), equation (19) becomes

$$\delta d_e^{\rm SSS} = \frac{13\hbar}{22RE_{\rm DC}}\frac{\xi_{\rm R}}{\sqrt{NTt_{\rm total}}}. \tag{20}$$

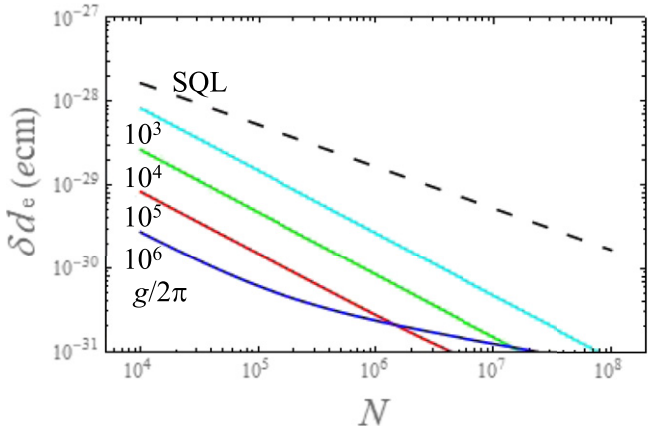

Figure 4. Dependence of the EDM uncertainty δd_e on N. The dashed line represents the δd_e with the SQL. Solid lines show δd_e in the SSS with the single-photon Rabi frequencies $2g$ ($g/2\pi$ of 10^3, 10^4, 10^5 and 10^6 Hz).

Now, we estimate the probability p in equation (11) to calculate equation (20). The spin flip with the probability p results from the photon scattering event in ^{210}Fr, there are two Raman processes with the π polarization probe light: (i) the transition from $|\uparrow\rangle = |7S_{1/2}, F = 13/2, M_F = 11/2\rangle$ to $|\downarrow\rangle = |7S_{1/2}, F = 11/2, M_F = 11/2\rangle$ via $|\mathrm{e}\rangle = |7P_{3/2}, F' = 13/2, M'_F = 11/2\rangle$. (ii) The transition from $|\uparrow\rangle$ to $|\downarrow\rangle$ via $|\mathrm{e}'\rangle = |7P_{3/2}, F' = 11/2, M'_F = 11/2\rangle$. We define the matrix element for the transition between $|F, m_F\rangle$ and $|F', m'_F\rangle$ as $M_{F,m_F,F\prime,m\prime_F}$. The Raman scattering rate [50] is proportional to $|M_{13/2,11/2,13/2,11/2}$ $M_{11/2,11/2,13/2,11/2} + M_{13/2,11/2,11/2,11/2}M_{11/2,11/2,11/2,11/2}|^2 = 0$. Therefore, the two Raman process are completely canceled. Next, we consider the Raman transition to the different magnetic sublevel. In fact, this process also increases $\Delta J'_z$ in equation (41) in reference [44]. We consider the transition from the $7S_{1/2}, F = 13/2, M_F = 11/2$ to $7S_{1/2}, F = 11/2, M_F = 9/2$ state via $|\mathrm{e}\rangle$ and $|\mathrm{e}'\rangle$. Then, $|M_{13/2,11/2,13/2,11/2}M_{11/2,9/2,13/2,11/2} + M_{13/2,11/2,11/2,11/2}M_{11/2,9/2,11/2,11/2}|^2 = 88/507$. In reference [44], this value should be divided by the single transition matrix element from the other state for rescaling. Therefore, we divided 88/507 by $|M_{11/2,11/2,13/2,11/2} + M_{11/2,11/2,11/2,11/2}|^2$. It gives $1/6.025$. The term including p due to Raman process to the other magnetic sublevel $|3\rangle$ in equation (41) in reference [44] is smaller than the first term in equation (41) by a factor of 4. Therefore, we obtain $p \sim 1/24$.

Figure 4 shows the estimated curve of uncertainty of eEDM δd_e using equations (19) and (20) with $E = 100$ kV cm^{-1}, $T = 1$ s, $t_{\mathrm{total}} = 24\mathrm{h} = 86\,400$ s, $\kappa/2\pi = 8$ kHz (corresponding to a finesse of 200 000 and cavity length L of 10 cm), $\Gamma/2\pi = 7.6$ MHz, and $\omega_a/2\pi = 46.8$ GHz for ^{210}Fr atoms. We assume $q = 1$. The dashed line represents the $\delta d_e^{\mathrm{CSS}}$ for SQL based on equation (19). The solid lines represents the $\delta d_e^{\mathrm{SSS}}$ based on equation (20) with $g/2\pi = 10^3, 10^4, 10^5, 10^6$ Hz. In the case of $g/2\pi = 10^5$ and 10^6 Hz, δd_e at $N = 1.8 \times 10^5$ is below $1 \times 10^{-30} e$cm. Figure 5 shows the δd_e as a function of $g/2\pi$ with $N = 10^2$, 10^3, 10^4, 10^5, 2.5×10^5 and 10^6. For increasing g, δd_e decreases. However, δd_e increases for higher g. Therefore, the minimum is reached at an optimal value of g. The curve reaches the minimum value with $\xi_{\mathrm{R}}^2 = \sqrt{16/(24q)}\ \Gamma/\omega_a$ at $NC = \frac{1}{4}(\omega_a/\Gamma)^2$ [44]. This is about 1/7500 for ^{210}Fr. Thus, $k \sim 7500$ is the theoretical maximum enhancement for ^{210}Fr. δd_e is improved by $\xi_{\mathrm{R}} \sim 1/87$ from the SQL. The best theoretical value for δd_e in figure 5 is $1.9 \times 10^{-31} e$cm with $N = 10^6$ and $g/2\pi = 4 \times 10^5$ Hz. Furthermore, substituting the current best values of $N = 2.5 \times 10^5$ for trapped Fr atoms [51] and $g/2\pi = 10^5$ Hz (reported for Rb [19]) into equation (20) gives $\xi_{\mathrm{R}} = 1/44.2$ and $\delta d_e = 7.5 \times 10^{-31} e$cm.

In a real experiment, several kinds of additional frequency shifts must be considered. These shifts result is systematic errors in the measurement of eEDM. In the next section, we discuss these additional frequency shifts and their cancellation.

3. Additional shifts and cancellation

3.1. DC Stark shift, AC Stark shift, and Zeeman shift

In this section, we discuss the possible energy shifts encountered by the atoms, in this case Fr atoms, during the eEDM measurement. We consider the ultracold ^{210}Fr atoms trapped in a one-dimensional optical lattice, as shown in figure 1(b). Thus, the atoms will see AC light shifts due to the applied laser. It also requires application of DC electric field and magnetic field resulting in DC Stark shift and Zeeman shift, respectively. Thus, the interaction Hamiltonian of the atom can be expressed as

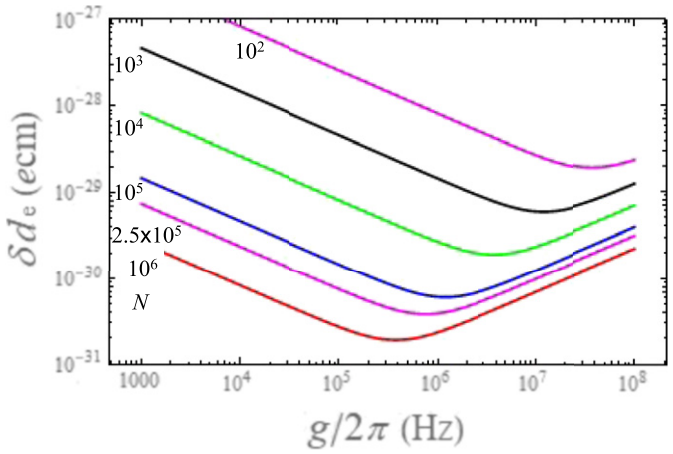

Figure 5. Dependence of EDM uncertainty δd_e on the single-photon Rabi frequency $2g$. Solid lines show the δd_e for the N of 10^2, 10^3, 10^4, 10^5, 2.5×10^5, and 10^6.

$$H = H_0 + H_{\text{EDM}} + H_{\text{DC Stark}} + H_{\text{light}} + H_{\text{Zeeman}}, \tag{21}$$

where H_0 is the unperturbed atomic Hamiltonian due to the electromagnetic interaction, H_{EDM} is the atomic EDM Hamiltonian, H_{DCStark} is the interaction Hamiltonian due to the DC electric field, H_{light} is the interaction Hamiltonian due to the AC electric field and H_{Zeeman} is the interaction Hamiltonian due to the magnetic field.

The DC Stark shift of a hyperfine level can be expressed as

$$\Delta E_{\text{DC Stark}} = -\frac{1}{2}\alpha_{F,M_F}(0)E_{\text{DC}}^2, \tag{22}$$

where E_{DC} is the static DC electric field and $\alpha_{F,M_F}(0)$ is known as the electric dipole ($E1$) polarizability of the corresponding hyperfine level. Since transitions between the hyperfine levels of the ground $7S$ state are considered in this analysis, the dominant second-order contributions to these levels will cancel out as they depend only on the angular momentum J values of the states, while the next leading-order due to the hyperfine induced contribution can contribute to the differential dipole polarizability.

The total dipole polarizability including the dominant second-order and the next leading-order hyperfine induced contributions can be given by

$$\alpha_{F,M_F}(0) = \alpha_F^{(2,0)}(0) + \alpha_F^{(3,0)}(0) + \frac{3M_F^2 - F(F+1)}{F(2F-1)}\alpha_F^{(3,2)}(0), \tag{23}$$

where $\alpha_F^{(2,0)}(0)$ is the second-order static $E1$ polarizability, and $\alpha_F^{(3,0)}(0)$ and $\alpha_F^{(3,2)}(0)$ are the scalar and tensor contributions to the third-order hyperfine mediated static $E1$ polarizabilities. In a sum-over-states approach, $\alpha_F^{(2,0)}(0)$ can be expressed as

$$\alpha_F^{(2,0)}(0) = -\frac{2}{3(2J+1)}\sum_k \frac{|\langle J\|\mathbf{D}\|J_k\rangle|^2}{E_0 - E_k}, \tag{24}$$

where $\langle J\|\mathbf{D}\|J_k\rangle$ are the reduced $E1$ matrix elements between the ground and other possible intermediate states k having angular momentum J_k. Here, E_0 is the ground state energy and E_k is the energy of the corresponding intermediate state k. To carry out the calculation conveniently, we categorise the contributions from the sum into low-lying valence states, high-lying valence states and occupied states. The low-lying valence states give the dominant contribution and are denoted as the 'main' contribution, contributions from the high-lying valence states are given as 'tail', while the contributions from the occupied states are given in two parts as 'core' and 'core–valence'. We use the $E1$ matrix elements from the singles and doubles approximated relativistic coupled-cluster theory (RCCSD method) together with experimental energies to estimate the 'main' contribution. To improve the accuracy of 'main', we use the precisely known $E1$ matrix elements of the $D1$ and $D2$ lines from reference [52]. The 'core–valence' and 'tail' contributions are estimated using the Dirac–Hartree–Fock method, while the 'core' is evaluated using the random phase approximation. We have also estimated the uncertainties for these quantities and obtain the final value for $\alpha_F^{(2,0)}(0)$ as 317.1(1.3) a.u.. We present the individual contributions to this quantity in

Table 1. Contributions from various E1 reduced matrix elements and other contributions to the second-order dipole scalar and vector E1 polarizabilities of the $F = 13/2$ and $F = 11/2$ hyperfine levels at $\omega = 0$ and $\omega = 0.031729$ a.u. ($\lambda = 1436$ nm). Our final value for the static dipole polarizability is compared with the previously reported results.

		$\omega = 0$	$\omega = 0.031\,729$ a.u.		
Transition	Reduced E1 matrix	$\alpha^{(2,0)}_{F=13/2;11/2}$	$\alpha^{(2,0)}_{F=13/2;11/2}$	$\alpha^{(2,1)}_{F=13/2}$	$\alpha^{(2,1)}_{F=11/2}$
		Main			
$7S_{1/2} - 7P_{1/2}$	4.277(8)	109.4(4)	161.7(6)	−184.1(7)	156.4(7)
$7S_{1/2} - 7P_{3/2}$	5.898(15)	182.8(9)	243.7(1.2)	121.9(6)	−103.6(6)
$7S_{1/2} - 8P_{1/2}$	0.34(1)	0.36(2)	0.40(2)	−0.24(1)	0.20(1)
$7S_{1/2} - 8P_{3/2}$	0.95(2)	2.8(1)	3.0(1)	0.90(4)	−0.76(4)
$7S_{1/2} - 9P_{1/2}$	0.11(1)	0.03(1)	0.03(1)	−0.02(0)	0.01(0)
$7S_{1/2} - 9P_{3/2}$	0.44(2)	0.52(5)	0.55(5)	0.14(1)	−0.12(1)
$7S_{1/2} - 10P_{1/2}$	0.05(0)	0.01(0)	0.01(0)	0.00(0)	0.00(0)
$7S_{1/2} - 10P_{3/2}$	0.26(1)	0.17(1)	0.18(1)	0.04(1)	−0.04(1)
$7S_{1/2} - 11P_{1/2}$	0.04(0)	0.0(0)	0.0(0)	0.00(0)	0.00(0)
$7S_{1/2} - 11P_{3/2}$	0.18(1)	0.08(1)	0.08(1)	0.02(0)	−0.02(0)
Total		296.10(99)	409.7(1.4)	−61.3(9)	52.1(9)
Tail		1.5(5)	1.3(7)	0.2(1)	−0.2(1)
Core–valence		−0.9(3)	−1.0(5)	∼0	∼0
Core		20.4(5)	28.2(6)	0.0	0.0
Final sum		317.1(1.3)	438.4(1.5)	−61.1(9)	52.6(9)
Others		316.81 [53] 289.8 [54] 315.2 [55] 317.8(2.4) [56]			

Table 2. Contributions from $\alpha_F^{(\mathrm{top},i=0,2)}(\omega)$, $\alpha_F^{(\mathrm{cen},i=0,2)}(\omega)$ and $\alpha_F^{(\mathrm{norm},i=0,2)}(\omega)$ to the $\alpha_F^{(3,0)}$, $\alpha_F^{(3,1)}$ and $\alpha_F^{(3,2)}$ values (in $\times 10^{-2}$ a.u.) of the $F = 13/2$ and $F = 11/2$ hyperfine levels of the ground state of ^{210}Fr at $\omega = 0$ and $\omega = 0.031729$ a.u. ($\lambda = 1436$ nm). The value can be converted from a.u. to SI unit by multiplying with the conversion factor $1/(4\pi\epsilon_0 a_0^3) = 0.248\,8319$ kHz $(\mathrm{kV\,cm^{-1}})^{-2}$ [61].

	$\omega = 0$		$\omega = 0.031\,729$ a.u.		
Contribution	$\alpha_F^{(3,0)}$	$\alpha_F^{(3,2)}$	$\alpha_F^{(3,0)}$	$\alpha_F^{(3,1)}$	$\alpha_F^{(3,2)}$
			***F* = 13/2level**		
$\alpha_F^{(\mathrm{top},i=0,2)}(\omega)$	1.2369	0.0455	1.7481	0.1358	0.0657
$\alpha_F^{(\mathrm{cen},i=0,2)}(\omega)$	0.0133	−0.1097	0.0501	0.5412	−0.3173
$\alpha_F^{(\mathrm{norm},i=0,2)}(\omega)$	1.6675	0.0	4.1464	1.5805	0.0
Final	2.9177	−0.0642	5.9446	2.2575	−0.2516
			***F* = 11/2level**		
$\alpha_F^{(\mathrm{top},i=0,2)}(\omega)$	−1.4431	−0.0321	−2.0394	0.1340	−0.0464
$\alpha_F^{(\mathrm{cen},i=0,2)}(\omega)$	−0.0155	0.0774	−0.0584	0.5342	0.2237
$\alpha_F^{(\mathrm{norm},i=0,2)}(\omega)$	−1.9454	0.0	−4.8375	1.5602	0.0
Final	−3.4030	0.0453	−.9353	2.2284	0.1773

table 1 and compare the final result with the previously reported values [53–56]. As can be seen, our result agrees with other values in literature and is also more precise.

The hyperfine induced $E1$ polarizability can be expressed as [57, 58, 60]

$$\alpha_F^{(3,i=0,2)}(0) = \alpha_F^{(\mathrm{top},i=0,2)}(0) + \alpha_F^{(\mathrm{cen},i=0,2)}(0) + \alpha_F^{(\mathrm{norm},i=0,2)}(0), \tag{25}$$

where $\alpha_F^{(\mathrm{top},i=0,2)}(0)$, $\alpha_F^{(\mathrm{cen},i=0,2)}(0)$ and $\alpha_F^{(\mathrm{norm},i=0,2)}(0)$ represent different static contributions, and their expressions can be found in references [57, 60]. We determine $\alpha_F^{(3,0)}$ and $\alpha_F^{(3,2)}$ values for the $F = 11/2$ and $F = 13/2$ hyperfine levels of the ground state of ^{210}Fr. Contributions from $\alpha_F^{(\mathrm{top},i=0,2)}(0)$, $\alpha_F^{(\mathrm{cen},i=0,2)}(0)$ and $\alpha_F^{(\mathrm{norm},i=0,2)}(0)$ to the third-order hyperfine induced scalar and tensor polarizabilities along with their final values of the above hyperfine levels are quoted in table 2. We have neglected contributions from the occupied and continuum orbitals in these estimations. As can be seen, the final values are much smaller than the $\alpha_F^{(2,0)}(0)$ values but they are more relevant to the present study.

Table 3. The DC Stark shifts $\omega^{J}_{\rm DC}/2\pi$ (MHz), $\omega^{F}_{\rm DC}/2\pi$ (kHz), and $\omega^{F,M}_{\rm DC}/2\pi$ (Hz) with $E = 100$ kV cm^{-1} in the hyperfine states of $7S_{1/2}$ in ^{210}Fr.

	$\omega^{J}_{\rm DC}/2\pi$ (MHz)	$\omega^{F}_{\rm DC}/2\pi$ (kHz)	$\omega^{F,M}_{\rm DC}/2\pi$ (Hz)
$F = 13/2$	−395.4	−36.800	30.7
$F = 11/2$	−395.4	42.705	−30.7

To measure the eEDM, we apply the MW field with a frequency resonant between the hyperfine levels $F = 13/2$ and $F = 11/2$. Therefore, the frequency shifts should be determined for each magnetic sublevel of these hyperfine states. Equation (22) can be rewritten as

$$\Delta E_{\rm DC\,Stark} \equiv \hbar\omega^{J}_{\rm DC} + \hbar\omega^{F}_{\rm DC} + \hbar\omega^{F,M}_{\rm DC} M_F^2 \tag{26}$$

with

$$\hbar\omega^{J}_{\rm DC} \equiv -\frac{1}{2}\alpha_F^{(2,0)}(0)E^2_{\rm DC}, \tag{27}$$

$$\hbar\omega^{F}_{\rm DC} \equiv -\frac{1}{2}\left(\alpha_F^{(3,0)}(0) - \frac{(F+1)}{(2F-1)}\alpha_F^{(3,2)}(0)\right)E^2_{\rm DC}, \tag{28}$$

$$\text{and} \quad \hbar\omega^{F,M}_{\rm DC} \equiv -\frac{3}{2F(2F-1)}\alpha_F^{(3,2)}(0)E^2_{\rm DC}, \tag{29}$$

where $\hbar\omega^{F}_{\rm DC}$ and $\hbar\omega^{F,M}_{\rm DC}$ are the M_F independent and dependent contributions, respectively, to the Stark shifts. These values are listed in table 3 for the $F = 11/2$ and $F = 13/2$ hyperfine levels.

Similarly, the light shift due to the AC electric field ($E_{\rm L}$) arising from the optical lattice can be expressed as

$$\Delta E_{\rm light} = -\frac{1}{2}\alpha_{F,M_F}(\omega)E^2_{\rm L}(\omega), \tag{30}$$

where $E_{\rm L}(\omega)$ is the electric field strength with angular frequency ω and $\alpha_{F,M_F}(\omega)$ is known as the dynamic $E1$ polarizability, given by

$$\alpha_{F,M_F}(\omega) = C_0(\alpha_F^{(2,0)}(\omega) + \alpha_F^{(3,0)}(\omega)) + C_1(\alpha_F^{(2,1)}(\omega) + \alpha_F^{(3,1)}(\omega)) + C_2\alpha_F^{(3,2)}(\omega). \tag{31}$$

$\alpha_F^{(i,0)}$, $\alpha_F^{(i,1)}$ and $\alpha_F^{(3,2)}$ are known as the scalar, vector and tensor polarizability contributions respectively for the second-order ($i = 2$) and third-order ($i = 3$) $E1$ polarizabilities. $C_{k=1,2,3}$ are coefficients whose values depend on the polarization of $E_{\rm L}$.

The dynamic second-order $E1$ polarizability can be evaluated by

$$\alpha_F^{(2,l=0,1)}(\omega) = \sum_k W_k^{(l=0,1)}\left[\frac{|\langle J\|\mathbf{D}\|J_k\rangle|^2}{E_0 - E_k + \omega} + (-1)^l\frac{|\langle J\|\mathbf{D}\|J_k\rangle|^2}{E_0 - E_k - \omega}\right] \tag{32}$$

with the coefficients

$$W_k^{(0)} = -\frac{1}{3(2J+1)}, \tag{33}$$

and

$$W_k^{(1)} = (-1)^{J_k+F+I+1}\sqrt{\frac{6F(2F+1)}{(F+1)}}\begin{Bmatrix} F & J & I \\ J & F & 1\end{Bmatrix}\begin{Bmatrix} J & 1 & J \\ 1 & J_k & 1\end{Bmatrix}. \tag{34}$$

These values for both the $F = 13/2$ and $F = 11/2$ hyperfine levels are given in table 1. Similarly, the third-order hyperfine interaction mediated dynamic $E1$ polarizabilities can be evaluated by

$$\alpha_F^{(3,i=0,1,2)}(\omega) = \alpha_F^{(\rm top,i=0,2)}(\omega) + \alpha_F^{(\rm cen,i=0,1,2)}(\omega) + \alpha_F^{(\rm norm,i=0,1,2)}(\omega), \tag{35}$$

where the expressions for $\alpha_F^{(\rm top,i=0,1,2)}(\omega)$, $\alpha_F^{(\rm cen,i=0,1,2)}(\omega)$ and $\alpha_F^{(\rm norm,i=0,1,2)}(\omega)$ can be found in references [57, 60], and these contributions to the scalar, vector and tensor parts for both the $F = 13/2$ and $F = 11/2$ hyperfine levels are given in table 2. The final values of the third-order $E1$ polarizabilities, after adding the above three contributions, are also given in the same table.

The coefficients for the linearly polarized light are given by [59]

$$C_0 = 1, \quad C_1 = 0, \quad \text{and} \quad C_2 = \frac{3M_F^2 - F(F+1)}{F(2F-1)} \tag{36}$$

Table 4. Estimated light shifts in the hyperfine levels of the $7S_{1/2}(F)$ in ^{210}Fr due to the light shifts $\omega^0_{\rm light}/2\pi$ (in MHz), $\omega^1_{\rm light}/2\pi$ (in kHz), and $\omega^2_{\rm light}/2\pi$ (in Hz) for the light with a wavelength of 1436 nm, power $P = 5$ W, a beam waist $w_0 = 50$ μm, and σ^+ and π polarizations.

F	$\hbar\omega^0_{\rm light}$	$\hbar\omega^1_{\rm light}$	$\hbar\omega^2_{\rm light}$
		πpolarization	
13/2	−4.889	0.0	1.155
11/2	−4.888	0.0	−1.155
		σ^+polarization	
13/2	−4.889	56.248	−5.773
11/2	−4.888	−56.522	−5.773

and for the circularly polarized light, they correspond to

$$C_0 = 1, \quad C_1 = \frac{AM_F}{2F}, \quad \text{and} \quad C_2 = -\frac{3M_F^2 - F(F+1)}{2F(2F-1)}, \tag{37}$$

where A is known as the degree of circular polarization and takes the values 1 and −1 for right-hand and left-hand circularly polarized electric field, respectively.

Using the above quantities, we can rewrite the light shift due to $E_{\rm L}$ as

$$\Delta E_{\rm light} \equiv \hbar\omega^0_{\rm light} + \hbar\omega^1_{\rm light} M_F + \hbar\omega^2_{\rm light} M_F^2, \tag{38}$$

where the first, second and third terms are the contributions independent of M_F, linear in M_F and quadratic in M_F respectively. The estimated $\hbar\omega^0_{\rm light}$, $\hbar\omega^1_{\rm light}$ and $\hbar\omega^2_{\rm light}$ values for the $F = 11/2$ and $F = 13/2$ levels are given in table 4.

Next, we intend to estimate the Zeeman shifts due to $H_{\rm Zeeman}$. To extract $\Delta\omega_{\rm EDM}$ from the frequency shifts due to the Hamiltonian of equation (20), it is necessary to apply an external magnetic field $\mathbf{B}_{\rm ext}$ parallel followed by anti-parallel to the external electric field $\mathbf{E}_{\rm DC}$. The typical magnitude of the applied external magnetic field $B_{\rm ext}$ is 200 pT. In addition, there is also a background magnetic field. The dominating ambient field is the earth's magnetic field which is of the order of $\sim 3 \times 10^{-5}$ T. Using compensation Helmholtz coils along the x, y, and z axes reduces this by a factor 100, and magnetic shields will give an additional reduction factor of 10^6 [62]. This would leave a residual magnetic field of the order of $\sim 3 \times 10^{-13}$ T, which is defined as $\mathbf{B}_{\rm res} \equiv \mathbf{B}_{\rm r,\parallel} + \mathbf{B}_{\rm r,\perp}$, where $\mathbf{B}_{\rm r,\parallel}$ and $\mathbf{B}_{\rm r,\perp}$ are the residual magnetic fields parallel and perpendicular to $\mathbf{E}_{\rm DC}$. If the direction of $\mathbf{E}_{\rm DC}$ and $\mathbf{B}_{\rm ext}$ is same, the energy shift $\Delta E_{\rm Zeeman}$ is written as [6]

$$\Delta E_{\rm Zeeman,\uparrow\uparrow} \equiv \hbar\omega_{0,\uparrow\uparrow} g_F M_F + \hbar\omega_1 K_1 g_F^2 + \hbar\omega_{2,\uparrow\uparrow} K_2 g_F^3, \tag{39}$$

$$\hbar\omega_{0,\uparrow\uparrow} \equiv -\mu_{\rm B}(B_{\rm ext} + B_{r,\parallel}) \tag{40}$$

$$\hbar\omega_1 \equiv \frac{\mu_{\rm B}^2 B_{r,\perp}^2}{\hbar\omega_{\rm DC}^{F,M}} \tag{41}$$

$$\hbar\omega_{2,\uparrow\uparrow} \equiv -\frac{\mu_{\rm B}^3 B_{r,\perp}^2 (B_{\rm ext} + B_{r,\parallel})}{(\hbar\omega_{\rm DC}^{F,M})^2}, \tag{42}$$

where the arrows in the subscripts signify that the directions of $\mathbf{E}_{\rm DC}$ and $\mathbf{B}_{\rm ext}$ are parallel. K_1 and K_2 are coefficients which are function of M_F [6]. K_1 has M_F^2 dependence whereas K_2 has M_F and M_F^2 dependence. Thus, although K_1 does not depend on the sign of M_F, K_2 does. Applying $\mathbf{B}_{\rm ext}$ opposite to the direction of $\mathbf{E}_{\rm DC}$ gives

$$\Delta E_{\rm Zeeman,\uparrow\downarrow} \equiv -\hbar\omega_{0,\uparrow\downarrow} g_F M_F + \hbar\omega_1 K_1 g_F^2 - \hbar\omega_{2,\uparrow\downarrow} K_2 g_F^3, \tag{43}$$

$$\hbar\omega_{0,\uparrow\downarrow} \equiv -\mu_{\rm B}(B_{\rm ext} - B_{r,\parallel}) \tag{44}$$

$$\hbar\omega_{2,\uparrow\downarrow} \equiv -\frac{\mu_{\rm B}^3 B_{r,\perp}^2 ((B_{\rm ext} - B_{r,\parallel})}{(\hbar\omega_{\rm DC}^{F,M})^2}. \tag{45}$$

In the above expressions, $\omega_{0,2,\uparrow\uparrow}$ ($\omega_{0,2,\uparrow\downarrow}$) indicates the Zeeman shift when $\mathbf{E}_{\rm DC}$ and $\mathbf{B}_{\rm ext}$ are parallel and anti-parallel respectively.

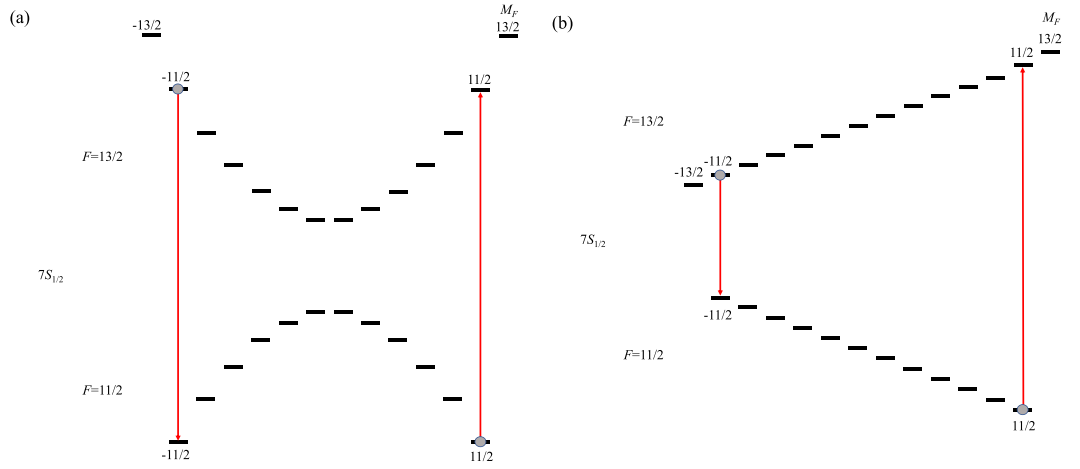

Figure 6. Energy diagram and MW transitions. (a)Tensor DC Stark shifts and tensor light shifts of magnetic sublevels in the hyperfine states of $7S_{1/2}$. (b) Zeeman shifts and vector light shifts of magnetic sublevels.

3.2. Cancellation of frequency shifts

We now consider the cancellation of the additional frequency shifts during the measurement. Figure 6(a) shows the M_F sublevel dependency of the $\omega_{\rm DC}^{F,M}M_F^2$ contribution to the DC Stark shift in equation (26). This is the dominant contribution and the other contributions to the DC Stark shift are omitted since $\omega_{\rm DC}^{J}$ and $\omega_{\rm DC}^{F}$ are not dependent on the magnetic sublevel. The diagram in figure 6(a) also includes the tensor light shift $\omega_{\rm light}^{2}$. After the second Ramsey MW pulse in the time sequence shown in figure 3(b), the z components of Bloch vectors measured as the Ramsey resonance are given by equations (12) and (13) including $\Delta\omega_{\pm M}$. Taking into account the additional frequency shift of equations (26), (38), (39) and (43), $\Delta\omega_{\pm M}$ in equation (15) can be replaced by

$$\begin{aligned}\Delta\omega_{\pm M} = {} & \omega_{\rm HFS} + \Delta\omega_{{\rm EDM},\pm M} + \Delta\omega_{\rm DC}^{F} + \Delta\omega_{\rm DC}^{F,M}M^2 \\ & + \Delta\omega_{\rm light}^{S} \pm \Delta\omega_{\rm light}^{V}M + \Delta\omega_{\rm light}^{T}M^2 \\ & + \Delta\omega_{{\rm Zeeman},\pm M} - \omega_{MW},\end{aligned} \tag{46}$$

where

$$\Delta\omega_{{\rm EDM},\pm M} \equiv \Delta\omega_{\rm EDM}^{\pm M,\pm M} \tag{47}$$

$$\Delta\omega_{\rm DC}^{F} \equiv \omega_{{\rm DC},F=13/2}^{F} - \omega_{{\rm DC},F=11/2}^{F} \tag{48}$$

$$\Delta\omega_{\rm DC}^{F,M} \equiv \omega_{{\rm DC},F=13/2}^{F,M} - \omega_{{\rm DC},F=11/2}^{F,M} \tag{49}$$

$$\begin{aligned}\Delta\omega_{{\rm light},\pm M}^{S} &\equiv (\omega_{{\rm light},F=13/2}^{0} - \omega_{{\rm light},F=11/2}^{0}) \\ \Delta\omega_{\rm light}^{V} &\equiv (\omega_{{\rm light},F=13/2}^{1} - \omega_{{\rm light},F=11/2}^{1}) \end{aligned} \tag{50}$$

$$\Delta\omega_{\rm light}^{T} \equiv (\omega_{{\rm light},F=13/2}^{2} - \omega_{{\rm light},F=11/2}^{2}) \tag{51}$$

$$\Delta\omega_{{\rm Zeeman},\pm M} \equiv \omega_0\frac{4}{13}M + \omega_2 K_2\frac{16}{2197}. \tag{52}$$

Here ω_0 is either $\omega_{0,\uparrow\uparrow}$ or $\omega_{0,\uparrow\downarrow}$. For ^{210}Fr, $g_F = 2/13$ for $F = 13/2$ and $g_F = -2/13$ for $F = 11/2$, and K_2 is proportional to the sign of M. Therefore, K_2 for M corresponds to $-K_2$ for $-M$ [6].

The signal S of equation (18) can accordingly be written as

$$\begin{aligned}S &\sim \frac{N}{2}(\Delta\omega_{+M} - \Delta\omega_{-M})T \\ &= \frac{N}{2}\left(\Delta\omega_{{\rm EDM},+M} - \Delta\omega_{{\rm EDM},-M} + 2\Delta\omega_{\rm light}^{V}M + \omega_0\frac{8}{13}M\right)T\end{aligned} \tag{53}$$

.

Equation (53) shows that the scalar DC Stark shift, tensor DC Stark shift, scalar light shifts, tensor light shift, and shift due to the frequency of MW field in the signal are all canceled out by the measurement scheme. It reduces the systematic errors due to the $\mathbf{E}_{\rm DC}$ and the lattice light. This cancellation can be

understood since the transition frequencies between $F = 13/2, M_F = 11/2 \rightarrow F = 11/2, M_F = 11/2$ and $F = 13/2, M_F = -11/2 \rightarrow F = 11/2, M_F = -11/2$ under the tensor DC Stark shift and tensor light shift are the same, as shown in figure 6(a). On the other hand, the transitions under the vector light shift and Zeeman shift (shown in figure 6(b)) remains in equation (53). Albeit the $\omega_{\rm MW}$ dependence is canceled, in order to maximize the excitation by the MW field, its frequency is tuned to $\omega_{\rm MW} = \omega_{\rm HFS} + \Delta\omega_{\rm DC}^{F} + \Delta\omega_{\rm DC}^{F,M}M^2 + \Delta\omega_{\rm light}^{S} + \Delta\omega_{\rm light}^{T}M^2$.

The vector light shifts for σ^- polarization is opposite to that for σ^+ polarization. As the polarization vector of the optical lattice beam is directed along y-axis, (thus it has the same amount of σ^+ and σ^- polarization components), the vector light shifts $\omega_{\rm light}^{V}$ are canceled. However, if the σ polarization component of the optical lattice light is slightly unbalanced, the cancellation will not be complete. Reducing the polarization purity to 10^{-5} results in the residual $\Delta\omega_{\rm light}^{V}/2\pi = 740$ mHz, as derived from table 4 with $P = 0.6$ W. In the following step, the measurement is pursued by reversing the direction of $\mathbf{E}_{\rm DC}$ and $\mathbf{B}_{\rm ext}$ to $-\mathbf{E}_{\rm DC}$ and $-\mathbf{B}_{\rm ext}$, respectively. As the polarity of σ polarization components are mirrored, due to the reversal of the quantization axis, the $\Delta\omega_{\rm DC}^{V}$ can be canceled by comparing the signal S for $\mathbf{E}_{\rm DC}$, $\mathbf{B}_{\rm ext}$ with that for $-\mathbf{E}_{\rm DC}$, $-\mathbf{B}_{\rm ext}$. In the event that the degree of circular handedness would change in a way that is correlated with the electric field reversal, a false eEDM signature may arise. To stem this source of a spurious signal, the polarization purity of optical lattice light, and its long term drifts and short term fluctuations, should be independently measured and characterized with atomic spectroscopy, for example the form of coherent population trapping and the detection of a dark state.

For this example, we assume a $B_{\rm ext}$ of 10 pT generated by Helmholtz coils with the current stabilized below 10^{-5}. The Zeeman shift $\omega_0\frac{8}{13}M/2\pi$ with $B_{\rm ext} = 200$ pT is 0.496 Hz. To cancel the Zeeman shifts, we reverse the direction of $\mathbf{B}_{\rm ext}$ relative to $\mathbf{E}_{\rm DC}$. Subtracting $S_{\uparrow\downarrow}$ from $S_{\uparrow\uparrow}$ cancels the $B_{\rm ext}$ terms in equations (39) and (43). However, the $B_{r,\parallel}$ terms remain, and at 3×10^{-13} T with the magnetic shield of 10^6 [62], the shift is about 0.014 Hz. The drift of earth magnetic field is typically 10^{-3} if there is no magnetic storm. Therefore, the fluctuation of residual magnetic field is 14 μHz inside the magnetic shield. During the Ramsey resonance measurement with $T = 1$ s, the SQL of frequency measurement is given by $1/(2\pi\sqrt{N}) = 0.318$ mHz for $N = 2.5 \times 10^5$. The Zeeman shifts in equation (53) during $T = 1$ s should be compensated with monitoring the magnetic field. Therefore, to independently estimate the background magnetic field $B_{r,\parallel}$, we propose measuring it using a spin-exchange relaxation free (SERF) magnetometer [63]. The sensitivity of the magnetometer can reach 7 fT $(\sqrt{\rm Hz})^{-1}$ at 1 Hz [64]. As the noise floor of the magnetometer corresponds to 98 μHz and the fluctuation of residual magnetic field from the earth magnetic field is 14 μHz as mention above, the drift of magnetic field is below the uncertainty of the magnetometer for $T = 1$ s. 98 μHz of the magnetometer is smaller than the SQL frequency uncertainty of 0.318 mHz for $T = 1$ s. In this way, the frequency shift $\Delta\omega_{{\rm EDM},+M} - \Delta\omega_{{\rm EDM},-M}$ in equation (53) with the uncertainty of 0.318 mHz is extracted and is compensated for the Zeeman shift of 0.496 Hz. Then, the integration of the frequency shift $\Delta\omega_{{\rm EDM},+M} - \Delta\omega_{{\rm EDM},-M}$ for $t_{\rm total} = 1$ day $= 86\,400$ s reduces the uncertainty of eEDM down to $3.3 \times 10^{-29}e$cm level.

In the case of the SSS, the SQL of frequency measurement with $\xi_{\rm R} = 1/44.2$ (as discussed in the end of section 2, $N = 2.5 \times 10^5$ for trapped Fr atoms [51], and $g/2\pi = 10^5$ Hz) gives 0.318 mHz/44.2 = 7.4 μHz. This is smaller than the noise floor of the magnetometer. On the other hand, the 16 magnetometers were used in the neutron EDM measurement [65]. Likewise, the uncertainty of 25 μHz for $T = 0.1$ due to the 16 SERF magnetometers is less than the uncertainty with the SSS of 74 μHz with the $T = 0.1$ s. To compare the uncertainty in the SSS with the CSS using $T = 1$ s and $t_{\rm total} = 1$ day, we consider $T = 0.1$ s and $t_{\rm total} = 10$ days for the SSS in order to keep the product of $Tt_{\rm total}$ in the equations (19) and (20). Then, equation (20) with $T = 0.1$ s and $t_{\rm total} = 10$ days gives $d_{\rm e} = 7.5 \times 10^{-31}e$cm as discussed in the section 2. Furthermore, the residual magnetic field that correlates with the electric field reversal should be checked by changing the magnitude of the electric field.

The $\mathbf{E} \times v$ effect has also been discussed in previously reported EDM measurements with atomic beam experiments [4, 66]. This term is added to the magnetic field. Laser cooling and trapping of atoms reduces the velocity, and thus, the effect. The mean values of the velocity $\mathbf{v}$ of atom in the optical lattice is about 9.2 mm s^{-1}. Then, $\mathbf{B} = \mathbf{v} \times \mathbf{E}_{\rm DC}/c^2 = 0.92$ pT. It corresponds to frequency shift of 0.81 mHz. However, as the velocity distribution of atoms trapped in the optical lattice is isotropic, the mean value of $\mathbf{v} \times \mathbf{E}_{\rm DC}/c^2$ is zero, and the dispersion remains.

After these estimates, the $\Delta\omega_{{\rm EDM},+M} - \Delta\omega_{{\rm EDM},-M} = 2\Delta\omega_{{\rm EDM},+M}$ can be obtained. This should be checked by changing the direction of $\mathbf{B}_{\rm ext}$, $\mathbf{E}_{\rm DC}$, switching the phase $\varphi = 0$ to π, changing the magnitude of $B_{\rm ext}$, and by changing the balance of $N_{F=13/2,M_F=-11/2}$ and $N_{F=11/2,M_F=+11/2}$. The quantum sensing using SSS may thus offer the potential to dramatically improve the resolution of the search for the eEDM to below $1 \times 10^{-30}e$cm. The large uncertainty will still bury the small difference. The large reduction of uncertainty by using SSS in experiment should also be useful for checking and reducing systematic errors generally.

4. Conclusion

We propose a method for measuring the eEDM arising from parity and time-reversal symmetry violations, using ultracold Fr atoms trapped in an optical lattice, with a potential uncertainty below the SQL. The dependence of the uncertainty in the EDM on a single-photon Rabi frequency inside the optical cavity is investigated. Quantum sensing using the SSS of a Fr atom for the measurement of its EDM is predicted to offer an uncertainty below 10^{-30} $e$cm. To estimate systematic uncertainties, we evaluated the DC Stark shifts due to the applied electric field, light shifts due to the optical lattice, and Zeeman shifts due to the applied magnetic field. We demonstrated that our proposed technique using the two Bloch vectors in the spin squeezed states cancel out the shifts arising from the Stark shifts due to both the DC field and the optical lattice in the measurement. This advocates for using the proposed quantum sensing technique to measure the eEDM, to a very low uncertainty. This technique can also be extended to measure the electric dipole moments of polar molecules. Thus, our proposed technique opens up a new possibility to carry out EDM measurements in the atomic systems as the next generation experiments to probe new physics beyond the SM of particle physics.

Acknowledgment

We thank Professor B P Das for many useful discussions. This work was supported by a Grant-in-Aid for Scientific Research (B) (No. 20H01929), and a Grant-in-Aid for Scientific Research (S) (No. 19H05601) from the Japan Society for the Promotion of Science (JSPS). BKS acknowledges access to the Vikram-100 HPC cluster of the Physical Research Laboratory (PRL), India for carrying out computations. The work of B A is supported by SERB-TARE(TAR/2020/000189), New Delhi, India.

Data availability statement

All data that support the findings of this study are included within the article (and any supplementary files).

ORCID iDs

T Aoki https://orcid.org/0000-0001-9875-2515
R Sreekantham https://orcid.org/0000-0002-4210-5922
B K Sahoo https://orcid.org/0000-0003-4397-7965
Bindiya Arora https://orcid.org/0000-0001-7083-034X
A Kastberg https://orcid.org/0000-0002-6175-2252
T Sato https://orcid.org/0000-0001-7699-8768
H Ikeda https://orcid.org/0000-0003-3229-6021
N Okamoto https://orcid.org/0000-0002-1295-7542
Y Torii https://orcid.org/0000-0002-7613-1344
T Hayamizu https://orcid.org/0000-0003-1966-7828
K Nakamura https://orcid.org/0000-0001-7773-1328
S Nagase https://orcid.org/0000-0001-7367-0062
M Ohtsuka https://orcid.org/0000-0002-1773-5711
H Nagahama https://orcid.org/0000-0001-7184-0267
N Ozawa https://orcid.org/0000-0002-5698-2133
M Sato https://orcid.org/0000-0003-1419-3192
T Nakashita https://orcid.org/0000-0002-6921-8556
K Yamane https://orcid.org/0000-0001-8460-6349
K S Tanaka https://orcid.org/0000-0001-6916-9654
K Harada https://orcid.org/0000-0002-5130-2848
H Kawamura https://orcid.org/0000-0002-2978-756X
T Inoue https://orcid.org/0000-0003-0505-5599
A Uchiyama https://orcid.org/0000-0001-9636-4631
A Hatakeyama https://orcid.org/0000-0002-0196-0375
A Takamine https://orcid.org/0000-0001-5528-7940
H Ueno https://orcid.org/0000-0003-4150-9500
Y Ichikawa https://orcid.org/0000-0001-5362-6523

Y Matsuda https://orcid.org/0000-0002-9847-3791
H Haba https://orcid.org/0000-0002-0170-8305
Y Sakemi https://orcid.org/0000-0001-8101-3900

References

[1] Safronova M S, Budker D, DeMille D, Kimball D F J, Derevianko A and Clark C W 2018 *Rev. Mod. Phys.* **90** 025008
[2] Cesarotti C, Lu Q, Nakai Y, Parikh A and Reece M 2019 *J. High Energy Phys.* JHEP05(2019)059
[3] ACME Collaboration 2018 *Nature* **562** 355
[4] Regan B C, Commins E D, Schmidt C J and DeMille D 2002 *Phys. Rev. Lett.* **88** 071805
[5] Murthy S A, Krause D, Li Z L and Hunter L R 1989 *Phys. Rev. Lett.* **63** 965
[6] Amini J M, Munger C T and Gould H 2007 *Phys. Rev.* A **75** 063416
[7] Shitara N, Yamanaka N, Sahoo B K, Watanabe T and Das B P 2021 *J. High Energy Phys.* JHEP02(2021)124
[8] Zhu K, Solmeyer N, Tang C and Weiss D S 2013 *Phys. Rev. Lett.* **111** 243006
[9] Parker R H *et al* 2015 *Phys. Rev. Lett.* **114** 233002
[10] Aoki T *et al* 2011 *Proc. 5th Int. Workshop on Fundamental Physics Using Atoms* ed ed N Sasao (Okayama, Japan: Okayama University)
[11] Kozyryev I and Hutzler N R 2017 *Phys. Rev. Lett.* **119** 133002
[12] The NL-eEDM Collaboration 2018 *Eur. Phys. J.* D **72** 197
[13] Sunaga A, Abe M, Prasannaa V S, Aoki T and Hada M 2020 *J. Phys. B: At. Mol. Opt. Phys.* **53** 015102
[14] Fitch N J, Lim J, Hinds E A, Sauer B E and Tarbutt M R 2021 *Quantum Sci. Technol.* **6** 014006
[15] Cairncross W B, Gresh D N, Grau M, Cossel K C, Roussy T S, Ni Y, Zhou Y, Ye J and Cornell E A 2017 *Phys. Rev. Lett.* **119** 153001
[16] Zhou Y *et al* 2020 *Phys. Rev. Lett.* **124** 053201
[17] Chin C, Leiber V, Vuletić V, Kerman A J and Chu S 2001 *Phys. Rev.* A **63** 033401
[18] Degen C L, Reinhard F and Cappellaro P 2017 *Rev. Mod. Phys.* **89** 035002
[19] Hosten O, Engelsen N J, Krishnakumar R and Kasevich M A 2016 *Nature* **529** 505
[20] Pedrozo-Peñafiel E *et al* 2020 *Nature* **588** 414
[21] Itano W M, Bergquist J C, Bollinger J J, Gilligan J M, Heinzen D J, Moore F L, Raizen M G and Wineland D J 1993 *Phys. Rev.* A **47** 3554
[22] Pezzè L, Smerzi A, Oberthaler M K, Schmied R and Treutlein P 2018 *Rev. Mod. Phys.* **90** 035005
[23] Kitagawa M and Ueda M 1993 *Phys. Rev.* A **47** 5138
[24] Takeuchi M, Ichihara S, Takano T, Kumakura M, Yabuzaki T and Takahashi Y 2005 *Phys. Rev. Lett.* **94** 023003
[25] Wineland D J, Bollinger J J, Itano W M, Moore F L and Heinzen D J 1992 *Phys. Rev.* A **46** R6797
[26] Wineland D J, Bollinger J J, Itano W M and Heinzen D J 1994 *Phys. Rev.* A **50** 67
[27] Riedel M F, Böhi P, Li Y, Hänsch T W, Sinatra A and Treutlein P 2010 *Nature* **464** 1170
[28] Kuzmich A, Bigelow N P and Mandel L 1998 *Europhys. Lett.* **42** 48
[29] Takahashi Y, Honda K, Tanaka N, Toyoda K, Ishikawa K and Yabuzaki T 1999 *Phys. Rev.* A **60** 4974
[30] Takano T, Fuyama M, Namiki R and Takahashi Y 2009 *Phys. Rev. Lett.* **102** 033601
[31] Appel J, Windpassinger P J, Oblak D, Hoff U B, Kjaergaard N and Polzik E S 2009 *Proc. Natl Acad. Sci.* **106** 10960
[32] Leroux I D, Smith M H S and Vuletić V 2010 *Phys. Rev. Lett.* **104** 073602
[33] Chen Z, Bohnet J G, Sankar S R, Dai J and Thompson J K 2011 *Phys. Rev. Lett.* **106** 133601
[34] Simsarian J E, Ghosh A, Gwinner G, Orozco L A, Sprouse G D and Voytas P A 1996 *Phys. Rev. Lett.* **76** 3522
[35] Lu Z-T, Corwin K L, Vogel K R, Wieman C E, Dinneen T P, Maddi J and Gould H 1997 *Phys. Rev. Lett.* **79** 994
[36] Atutov S N *et al* 2003 *J. Opt. Soc. Am.* B **20** 953
[37] Tandecki M, Zhang J, Collister R, Aubin S, Behr J A, Gomez E, Gwinner G, Orozco L A and Pearson M R 2013 *J. Instrum.* **8** P12006
[38] Harada K 2019 *11th Int. Workshop on Fundamental Physics Using Atoms (FPUA)* (Okinawa, Japan)
[39] Byrnes T M R, Dzuba V A, Flambaum V V and Murray D W 2016 *Phys. Rev.* A **59** 3082
[40] Schleier-Smith M H, Leroux I D and Vuletić V 2010 *Phys. Rev.* A **81** 021804(R)
[41] See appendix A Vrijsen G 2011 *PhD Thesis* Stanford University
[42] Saffman M, Oblak D, Appel J and Polzik E S 2009 *Phys. Rev.* A **79** 023831
[43] Nielsen A E B and Mølmer K 2008 *Phys. Rev.* A **77** 063811
[44] Chen Z, Bohnet J G, Weiner J M, Cox K C and Thompson J K 2014 *Phys. Rev.* A **89** 043837
[45] Cox K C, Greve G P, Weiner J M and Thompson J K 2016 *Phys. Rev. Lett.* **116** 093602
[46] Schleier-Smith M H, Leroux I D and Vuletić V 2010 *Phys. Rev. Lett.* **104** 073604
[47] Vuletić V, Chin C, Kerman A J and Chu S 1998 *Phys. Rev. Lett.* **81** 5768
[48] Drever R W P, Hall J L, Kowalski F V, Hough J, Ford G M, Munley A J and Ward H 1983 *Appl. Phys.* B **31** 97
[49] Zhang H, McConnell R, Ćuk S, Lin Q, Schleier-Smith M H, Leroux I D and Vuletić V 2012 *Phys. Rev. Lett.* **109** 133603
[50] Dörscher S, Schwarz R, Masoudi A A, Falke S, Sterr U and Lisdat C 2018 *Phys. Rev.* A **97** 063419
[51] Collister R *et al* (FrPNC Collaboration) 2014 *Phys. Rev.* A **90** 052502
[52] Simsarian J E, Orozco L A, Sprouse G D and Zhao W Z 1998 *Phys. Rev.* A **57** 2448
[53] Singh S, Sahoo B K and Arora B 2016 *Phys. Rev.* A **94** 023418
[54] Dammalapati U, Harada K and Sakemi Y 2016 *Phys. Rev.* A **93** 043407
[55] Lim I S, Schwerdtfeger P, Metz B and Stoll H 2005 *J. Chem. Phys.* **122** 104103
[56] Derevianko A, Johnson W R, Safronova M S and Babb J F 1999 *Phys. Rev. Lett.* **82** 3589
[57] Beloy K 2009 *PhD Thesis* University of Nevada, Reno
[58] Beloy K, Derevianko A, Dzuba V A and Flambaum V V 2009 *Phys. Rev. Lett.* **102** 120801
[59] Manakov N L, Ovsiannikov V D and Rapoport L P 1986 *Phys. Rep.* **141** 319
[60] Yu Y-M and Sahoo B K 2017 *Phys. Rev.* A **96** 050502(R)
[61] Mitroy J, Safronova M S and Clark C W 2010 *J. Phys. B: At. Mol. Opt. Phys.* **43** 202001
[62] Budker D, Yashchuk V and Zolotorev M 1998 *Phys. Rev. Lett.* **81** 5788

[63] Kominis I K, Kornack T W, Allred J C and Romalis M V 2003 *Nature* **422** 596
[64] Dang H B, Maloof A C and Romalis M V 2010 *Appl. Phys. Lett.* **97** 151110
[65] Abel C *et al* 2020 *Phys. Rev.* A **101** 053419
[66] Commins E D, Ross S B, DeMille D and Regan B C 1994 *Phys. Rev.* A **50** 2960